



**20<sup>th</sup> IAEA Fusion Energy Conference**  
**Vilamoura, Portugal, 1-6 November 2004**

---

**IAEA-CN-116/FT/P7-7**

# **Critical $\beta$ Analyses with Ferromagnetic and Plasma Rotation Effects and Wall Geometry for a High $\beta$ Steady State Tokamak**

**G. Kurita, J. Bialek#, T. Tuda, M. Azumi, S. Ishida, G.A. Navratil#, S. Sakurai,  
H. Tamai, M. Matsukawa, T. Ozeki, M.S. Chu\*, M.S. Chance†, Y. Miura**

**Naka Fusion Research Establishment, Japan Atomic Energy Research Institute,  
801-1 Mukoyama, Naka-machi, Naka-gun, Ibaraki-ken, Japan 311-0193**

**# Columbia University**

**\* General Atomics**

**† Princeton Plasma Physics Laboratory**

**e-mail contact of main author: kurita@naka.jaeri.go.jp**

---

This is a preprint of a paper intended for presentation at a scientific meeting. Because of the provisional nature of its content and since changes of substance or detail may have to be made before publication, the preprint is made available on the understanding that it will not be cited in the literature or in any way be reproduced in its present form. The views expressed and the statements made remain the responsibility of the named author(s); the views do not necessarily reflect those of the government of the designating Member State(s) or of the designating organization(s). In particular, neither the IAEA nor any other organization or body sponsoring this meeting can be held responsible for any material reproduced in this preprint.

## Critical $\beta$ Analyses with Ferromagnetic and Plasma Rotation Effects and Wall Geometry for a High $\beta$ Steady State Tokamak

G. Kurita, J. Bialek#, T. Tuda, M. Azumi, S. Ishida, G.A. Navratil#, S. Sakurai,  
H. Tamai, M. Matsukawa, T. Ozeki, M.S. Chu\*, M.S. Chance†, Y. Miura  
Naka Fusion Research Establishment, Japan Atomic Energy Research Institute,  
801-1 Mukoyama, Naka-machi, Naka-gun, Ibaraki-ken, Japan 311-0193

# Columbia University

\* General Atomics

† Princeton Plasma Physics Laboratory

e-mail contact of main author : kurita@naka.jaeri.go.jp

**Abstract.** The critical beta is shown to be decreased by ferromagnetic effect by about 8% for  $\mu/\mu_0 \sim 2$ ,  $\mu$  and  $\mu_0$  denote the permeability of ferromagnetic wall and vacuum, respectively, for tokamak of aspect ratio 3. The existence of the stability window opened by both effects of the toroidal plasma rotation and the plasma dissipation, which was not observed for high aspect ratio tokamak, is found for tokamak of aspect ratio 3. The effect of ferromagnetism on them is also investigated. The critical beta analyses of NCT (National Centralized Tokamak) plasma using VALEN code are started with stabilizing plate and vacuum vessel geometry with finite resistivity, and the results for passive effect of stabilizing plate are obtained. The calculations including stabilizing effect of the vacuum-vessel and also active feedback control are also performed for present design of NCT plasma.

### Introduction

In order to improve economic and environmental suitability of tokamak fusion reactors, both the accomplishment of high beta plasmas and the practical use of reduced activation materials to reduce the amount of radioactive waste are crucially important [1]. To obtain steady state of high beta tokamak plasma for economical fusion reactor, it is said that the resistive wall mode (RWM) [2-5], is one of the most dangerous MHD mode that must be controlled and/or stabilized. RWM is considered to be able to be stabilized by active feedback control, because its growth rate is slowed down to that of resistive wall time scale from usual much faster Alfvén time scale of external kink modes. This feedback stabilization of RWM with plasma rotation has been minutely investigated experimentally [6-9], theoretically and numerically [10-13]. Although low radio-activation ferritic steel is considered as a most promising candidate for structural material in DEMO reactors, the influence of a ferromagnetic property in the ferritic steel on MHD stability and beta limits has been poorly investigated so far [14,15]. The critical beta was shown to be decreased by ferromagnetic effect by about 10% for  $\mu/\mu_0 \sim 2$ ,  $\mu$  and  $\mu_0$  denote the permeability of ferromagnetic wall and vacuum, respectively, for high aspect ratio tokamak [15]. The existence of the stability window opened by both effects of the toroidal plasma rotation and the plasma dissipation for standard spect ratio tokamak [2, 3] was not observed for high aspect ratio tokamaks [15]. Although the plasma cross section is almost circular, we carried out the critical beta analyses for the equilibrium with aspect ratio,  $A=3$ , which fits the parameter of NCT facility [16]. NCT is planned to establish the high beta steady state operation and to ensure plasma applicability of ferritic steel as reduced activation material.

The effect of real geometry of stabilizing plate is also an important issue, and using VALEN code [17] we started to investigate the critical beta of NCT plasma with stabilizing plate and vacuum vessel geometry with finite resistivity. The numerical results including passive effects of stabilizing plate and vacuum-vessel and also the effect of active feedback control are obtained for present design of NCT.

### 1. Critical $\beta$ analysis with ferromagnetism

In this section, the MHD stability analyses are carried out using the linear MHD code, AEOLUS-FT, based on the original resistive MHD equations developed at JAERI. The code can include both the ferromagnetic and resistive wall effects with background plasma flow on external kink mode. The linearized resistive MHD equations using simplified Ohm's law with plasma flow and the effect of non-uniform permeability are shown below,

$$\begin{aligned}\rho_0 \frac{\partial \vec{v}}{\partial t} &= -\rho_0 (\vec{v}_0 \cdot \vec{\nabla}) \vec{v} - \vec{\nabla} p + (\vec{j}_0 \times \vec{b}) + (\vec{\nabla} \times (\vec{b} / \hat{\mu}) \times \vec{b}_0), \\ \frac{\partial \vec{b}}{\partial t} &= \vec{\nabla} \times (\vec{v}_0 \times \vec{b} + \vec{v} \times \vec{b}_0 - \eta \vec{\nabla} \times (\vec{b} / \hat{\mu})), \\ \frac{\partial p}{\partial t} &= -(\vec{v}_0 \cdot \vec{\nabla}) p - (\vec{v} \cdot \vec{\nabla}) p_0 - \Gamma p_0 \vec{\nabla} \cdot \vec{v}.\end{aligned}$$

Here,  $\rho$ ,  $v$ ,  $b$ ,  $p$  and  $\eta$  denote plasma density, plasma velocity, magnetic fields, plasma pressure and plasma resistivity, respectively, and subscript 0 denotes the equilibrium quantity,  $\hat{\mu}$  ( $=\mu/\mu_0$ ) is relative permeability and  $\Gamma$  is the specific heat ratio. Applicability and accuracy of AEOLUS-FT code for fixed-boundary problem were confirmed by a benchmark test with the FAR code developed at ORNL [18]. Dependence of the growth rate of the tearing mode against  $\beta_p$  was compared in two codes for circular tokamak plasma with aspect ratio of 10, and the excellent agreement was obtained [19]. To analyze the external kink mode in the AEOLUS-FT code, the "pseudo-vacuum" model [20, 21], where the vacuum is replaced by highly resistive plasma, is used instead of "real vacuum". The resistive wall including the effect of ferromagnetism is assumed to surround the plasma uniformly and the distance between the wall and the plasma is also uniform. In the following calculations, used are, unless otherwise noted, a circular plasma cross section and aspect ratio,  $A=3$ , the minor radius of resistive wall  $r_w=1.2a$ ,  $a$  is plasma minor radius, the thickness of the wall  $d=0.05a$  and a resistivity of the wall  $\eta_w=10^{-4}$ . The poloidal mode numbers are taken into account from  $m=-2$  up to  $m=13$ . The number of non-uniform grid points in the minor radius direction is typically 2501. Under the above conditions with almost parabolic current and pressure profiles, the dependence of the  $n=1$  mode growth rate on the normalized beta is obtained, where the permeability in the resistive wall is changed from  $\mu/\mu_0=1$  to 5. As shown in Fig.1, the growth rates clearly increase with the increase of the permeability and the critical normalized beta values are substantially reduced down to 92% at  $\mu=2\mu_0$ , 80% at  $\mu=5\mu_0$  in comparison with that at  $\mu=\mu_0$ . The reduction of normalized beta is estimated at the transition region from kink

mode to RWM,  $\gamma\tau_{pa}\approx 10^{-2}$  ( $\tau_{pa}$ : poloidal Alfvén time), shown by broken line in the figure.

## 2. Effect of ferromagnetism on stability window and plasma rotation

The effect of relative permeability on the stability window opened by effects of toroidal plasma rotation and sound wave damping term is shown in Fig.2 by growth rates of the closed symbols for  $V_{\phi}=0.5V_{pA}$  ( $V_{pA}$ : poloidal Alfvén velocity). The dotted region in the figure denotes the unstable region of ideal kink mode. The stability window is opened for  $V_{\phi}\geq 0.5V_{pA}$ , because curve of the growth rates crosses zero in the ideal kink unstable region for  $V_{\phi}=0.4V_{pA}$ . Increment of mode rotation frequency shown by open symbols in the figure and reduction of the width of stability window tend to become larger for higher values of relative permeability as seen in the case of  $\mu=5\mu_0$ . It is found that the maximum rotation frequency in the RWM unstable region tends to be increased as the unstable region is enlarged with increasing relative permeability. The permeability decouples two branches, which are coupled by the effects of toroidal plasma rotation and ion sound wave damping through toroidal effect, and mode rotation frequency becomes increasing function of the wall radius, which is a different tendency from the case without permeability,  $\mu=\mu_0$  [2]. It is suggested from the analysis that more careful phase control would be required for active feedback control for RWM with ferromagnetic wall. In these calculations, we use the values of a resistivity of the wall  $\eta_w=3\times 10^{-6}$ , and the value of the strength of sound wave damping term is chosen as 0.01.

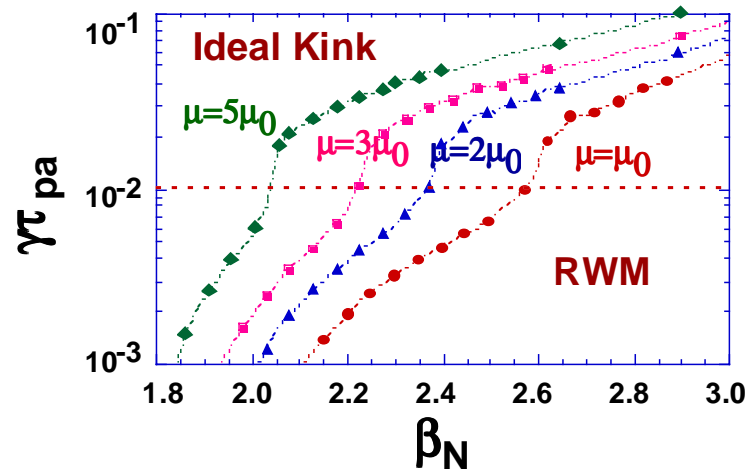


FIG.1 Normalized beta dependence of growth rate for four values of relative permeability. Broken line represents the transition boundary from RWM to ideal kink mode.

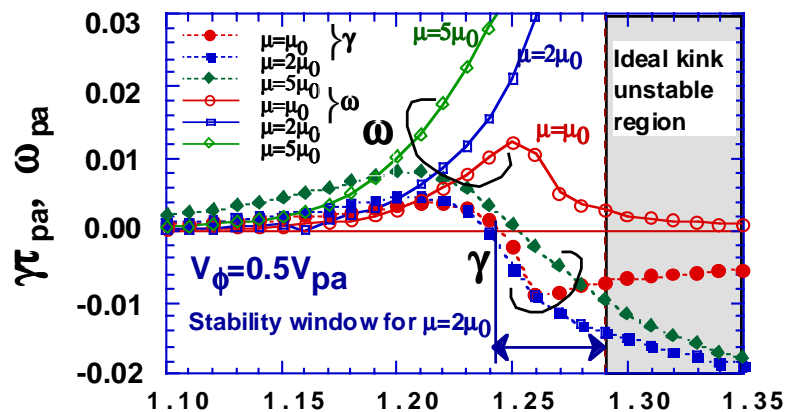


FIG.2 Growth rate and mode frequency as a function of the normalized wall radius for three relative permeability where the toroidal rotation velocity is 0.5 times poloidal Alfvén velocity.

In these calculations, we use the values of a resistivity of the wall  $\eta_w=3\times 10^{-6}$ , and the value of the strength of sound wave damping term is chosen as 0.01.

### 3. 3D analyses for stability and control

Critical normalized beta with the effect of the stabilizing structure and the active feedback control in real the NCT facility. The analyses are carried out by using VALEN code, and we first make the bench mark test between VALEN (DCON) and ERATO calculations. The typical equilibrium for up-down symmetric double-null NCT plasma, following stability calculations, is shown in Fig.3 for normalized beta of 3. Obtained two critical normalized beta values calculated by DCON and ERATO versus minor radius of the conformal ideal wall shows a good agreement.

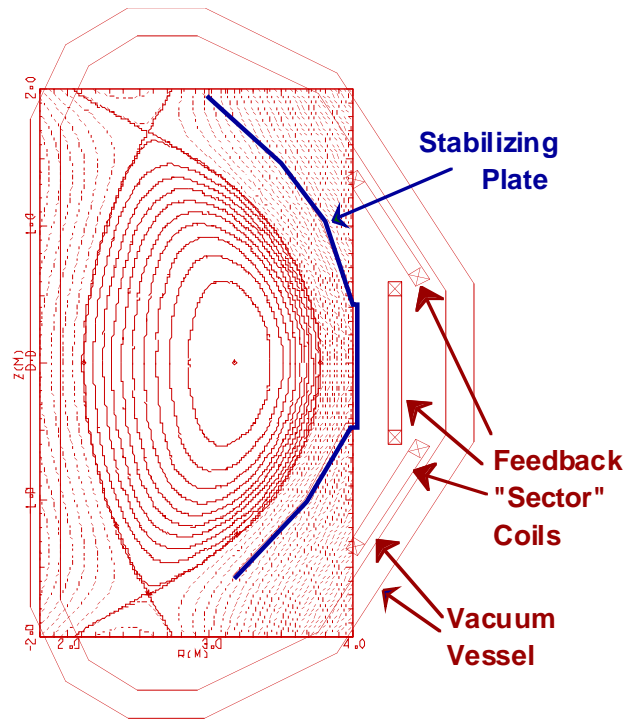


FIG.3 Typical up-down symmetric double-null equilibrium of NCT plasma for  $\beta_N=5$ . Stabilizing plate, double wall vacuum vessel and feedback "sector" coils are also shown.

Figure 4 shows the growth rates as a function of normalized beta obtained by VALEN code. The real structured, with the penetrations (portholes and edge cut outs), and idealstructured, without those, stabilizing plate are used in these calculations. The maximum increase of growth rate becomes more than 5 times larger due to the penetrations in stabilizing plate. Typical eddy current patterns induced by RWM on the stabilizing plate for (a) ideal case with hole and edge cut outs and (b) real case without them are shown in Fig.5. The distortion of eddy current pattern reduces the passive stabilization effect, and the growth rate increases. The growth rates are further increased by considering phase shift between

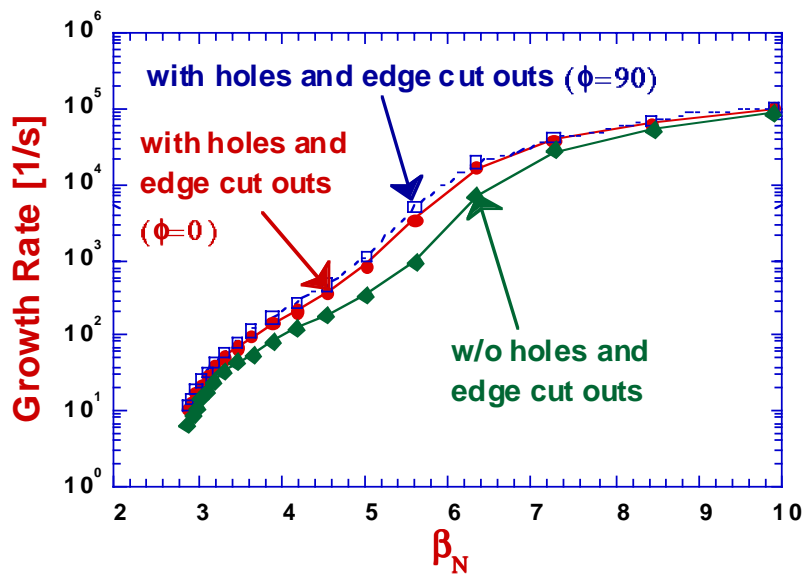


FIG.4 Growth rate versus normalized beta value for NCT plasma. Closed circles and closed squares denote the growth rate with and without holes and edge cut outs in stabilizing plate. Phase shift between mode and holes and edge cut outs in stabilizing plate is also considered (open squares).

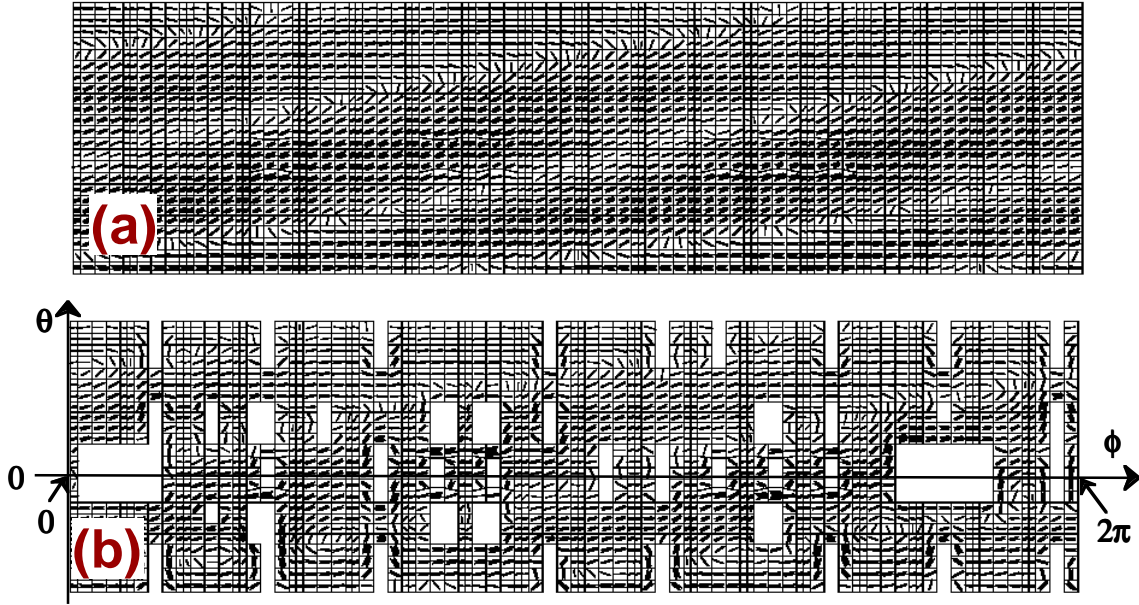


FIG.5 Eddy current pattern on the expanded stabilizing plate for (a) ideal case without holes and edge cut outs and (b) real case with holes and edge cut outs. Shape and place of holes and edge cut outs are shown in Fig.(b).  $\theta$  and  $\phi$  are poloidal and toroidal angles, respectively.

mode and holes and edge cut outs in stabilizing plate. The following analyses by VALEN code include the passive effect of single-wall vacuum vessel and the active control using 18 (6 toroidal and 3 poloidal directions) feedback coils, which we call “sector coils”. The sector coils are currently planned to be installed on the back of the stabilizing plate, and each coil is planned to have 20 kAT current with 10~20 Hz frequency range.

In the following, the calculations will include the passive effect of the vacuum vessel in addition to the stabilizing plate. Figure 6 illustrates the results of a VALEN calculation that compared the effects of different models of the vacuum vessel on the passive growth rate of the plasma instability. The following three models are compared firstly without the interior passive structure of stabilizing plate : the vacuum vessel is modeled as two independent toroidal shells without penetrations, 2) the vacuum vessel is modeled as a single toroidal shell, located at the position of the inner wall, with a thickness equal to the sum of the two walls, and 3) the vacuum vessel is modeled as a single toroidal shell, located at the position of the inner wall, having a wall thickness equal to the sum of the two walls, and all major radial penetrations are modeled. Only small differences in growth rate is observed among these three models. In the figure, the growth rate with the effect of the interior passive structure of stabilizing plate is also shown by lower two curves. The upper curve illustrates the passive growth rate typical of the interior passive structure alone and the lowest curve illustrates the passive growth rate in the case combined with the effect of single wall toroidal shell with penetrations. As expected, the passive structure provides most of the passive stabilization and the vacuum vessel wall is a secondary effect. In the following, therefore, only a single wall model of the vacuum vessel will be considered. We also ignore the mechanical connections between the stabilizing plate and the vacuum vessel in this paper, because the effect is considered to be small. Cut away view of stabilizing plate, single wall vacuum vessel and feedback (sector) coils of NCT facility, used in the calculation, are shown in Fig.7, where both

penetrations of these two passive structures are shown.

We finally try to predict the performance of the current designed active feedback system, where “sector coils” are planned to be installed on the back of the stabilizing plate. We use a ‘mode control’ feedback, where several poloidal field sensors are placed on the device mid plane inside the stabilizing plate. The axis of each of these sensor coils is in the vertical direction. The 18 control coils were connected as nine pairs. Each coil pair consists of diametrically

opposed coils (located at the same vertical position) being connected in anti series. A preliminary calculation is then run where all the coils are treated like sensors and a VALEN passive growth rate calculation is performed. The flux in all mid plane sensors and in all coil pairs is thus obtained. By examining the flux patterns in these different coils, we identify the relative phasing among the control coil pairs that would best couple to the plasma mode. We then specify a feedback relation; so that a voltage would be applied to each coil pair that is the product of proportional gain, max sensor flux, and phase factor, i.e.,

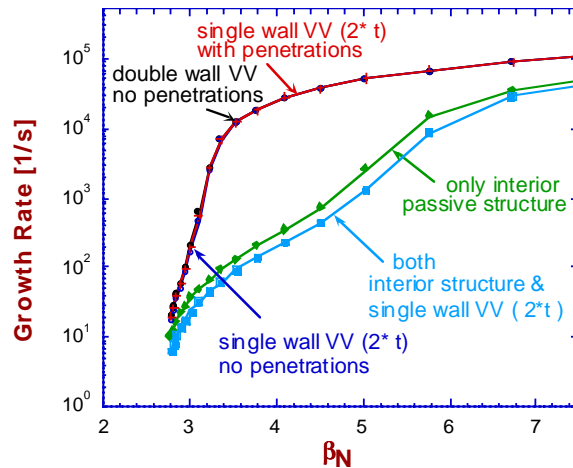


FIG.6 Passive growth rate versus normalized beta for different vacuum vessel models. Lower two curves illustrate the case with interior passive structure, stabilizing plate.

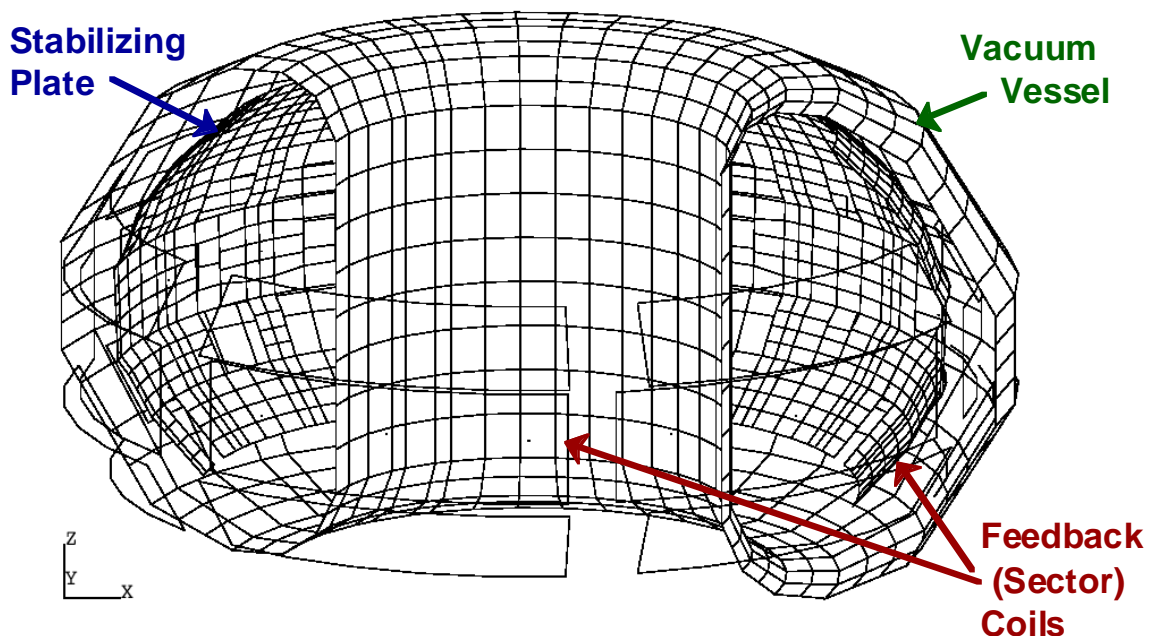


FIG.7 Cut away view of stabilizing plate, single wall vacuum vessel and feedback (sector) coils of NCT facility. The poloidal cross sectional views of these structures is shown in Fig.3. Penetration for both stabilizing plate and vacuum vessel is shown, but the mechanical connections between these two structures are ignored. Expanded view of stabilizing plate with holes and edge cut outs is shown in Fig.5(b).

$$V_{coil} = G_p (\Phi_{sensor})(\text{phase factor})$$

We refer to  $G_p$  as proportional gain. Since the area of each sensor is  $10^{-4}$  m<sup>2</sup> a measured poloidal field of 1 gauss ( $10^{-4}$  T) must be multiplied by a gain of  $10^8$  [volt/weber] to obtain a voltage of 1 volt. The following calculations will be carried out with single turn coils and single turn sensors for simplicity. The phase factor is also ignored in the following calculations.

Figure 8 illustrates the performance of the active feedback system in terms of normalized beta  $\beta_n$ .

The dashed line with closed circles shows the typical performance for passive stabilization, while the solid line with closed triangles shows the performance for ideal passive stabilization, where the sufficient low resistivity of the passive structure is used. From the curve of ideal wall case, the maximum critical normalized value for this model of passive structure and equilibria of NCT is estimated to be about 5.5. Other three curves, in the figure, illustrate the performance of the VALEN model when proportional gain  $G_p$  is set to respectively  $10^7$ ,  $10^8$ , and  $10^9$ . To the left of the approximate zero crossing the plasma instability has been successfully suppressed. For this model and plasma instability, we find best performance near  $G_p=10^8$  [volt/weber]. The estimated maximum normalized beta value is 3.8 using the proposed active feedback system, where “sector coils” are installed on the back of the stabilizing plate. The performance of the proposed feedback system is not so good, and the design of the shape and position of “sector coils” are being changed to be embedded in horizontal port holes to improve the response time of feedback fields to the plasma, just the same as in FIRE design. By this change, the critical normalized beta value will be much increased.

#### 4. Conclusion

In conclusion, the presence of ferromagnetic wall effect is identified as the critical beta is reduced to 92% of that without ferromagnetism with a wall thickness of  $0.05a$  for  $\mu/\mu_0=2$  at which the permeability value is sufficiently saturated. It is found that the maximum rotation frequency in the RWM unstable region tends to be increased as the unstable region is enlarged with increasing relative permeability. The critical beta analyses of NCT plasma using VALEN code are performed with stabilizing plate and vacuum vessel geometry with finite resistivity, and it is shown that the passive plate provides most of the passive stabilization and the vacuum vessel wall is a secondary effect. The active feedback control analyses using current designed active feedback system, where “sector coils” are planned to

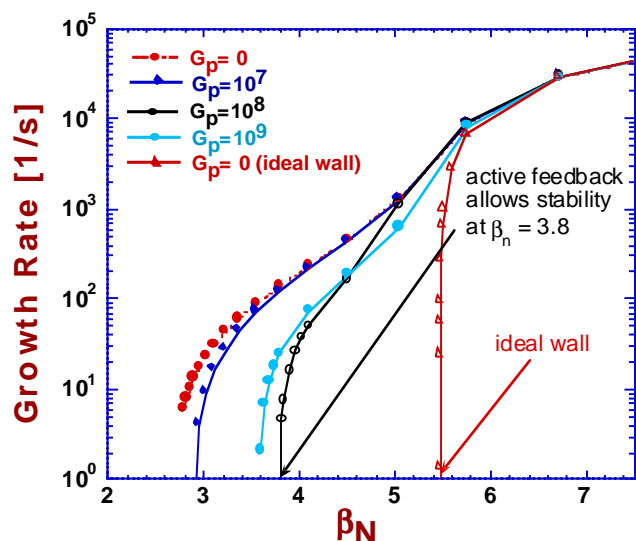


FIG.8 Growth rate versus normalized beta for different proportional gain  $G_p$ . Dashed curve with closed circles and solid curve with opened triangles ( $G_p=0$ ) show the case with only effect of passive stabilizing structure with finite resistivity and no resistivity, respectively.

be installed on the back of the stabilizing plate, is also carried out, and the maximum normalized beta value of 3.8 is obtained.

### Acknowledgments

The authors would like to express their sincere thanks to Dr. M. Kikuchi for his arrangement of the collaboration with Columbia University. They also want to acknowledge to Drs. H. Ninomiya and M. Nagami for their useful comments and encouragement.

This work was partly supported by JSPS, Grant-in-Aid for Scientific Research (C) No.15560720.

### References

- [1] Seki, Y., et al., Proc. 13<sup>th</sup> IAEA Conf. on Controlled Nuclear Fusion and Plasma Physics, Washington, 1990, IAEA-CN-53/G-1-2.
- [2] Bondeson, A., and Ward, D. J., Phys. Rev. Lett., 72, (1994) 2709.
- [3] Chu, M.S., Greene, J.M., Jensen, T.H., et al., Phys. Plasmas 2, (1995) 2236.
- [4] Finn, J.M., Phys. Plasmas, 2, (1995) 198.
- [5] Betti, R., Phys. Plasmas, 5, (1998) 3615.
- [6] Strait, E.J., Taylor, T.S., Turnbull, A.D., et al., Phys. Rev. Lett., 74, (1995) 2483.
- [7] Garofalo, A.M., Jensen, T.H., Johnson, L.C., et al., Phys. Plasmas, 9, (2002) 1997.
- [8] Navratil, G.A., Bialek, J., Boozer, A.H., et al., in Plasma Physics and Controlled Nuclear Fusion Research 2000 (Proc. 18th Int. Conf. Sorrent, 2000), CD-ROM file EXP3/16(R).
- [9] Garofalo, A.M., Chu, M.S., Fredrickson, E.D., et al., Nucl. Fusion, 41, (2001) 1171.
- [10] Okabayashi, M., Pomphrey, N., and Hatcher, R.E., Nucl. Fusion, 38, (1998) 1607.
- [11] Liu, Y.Q., and Bondeson, A., Phys. Rev. Lett., 84, (2000) 907.
- [12] Okabayashi, M., Bialek, J., Chance, M.S., et al., Plasma Phys. Control. Fusion, 44, (2002) B339.
- [13] Chu, M.S., Chan, V.S., Chance, M.S., et al., Nucl. Fusion, 43, (2003) 196.
- [14] Gimblett, C.G., Nucl. Fusion, 26, (1986) 617.
- [15] Kurita, G., Tuda, T., Azumi, M., et al., Nucl. Fusion 43, (2003) 949.
- [16] Ishida, S., et al., Nucl. Fusion 43, (2003) 606.
- [17] Bialek, J., Boozer, A.H., Mauel, M.E., and Navratil, G.A., Phys. Plasmas, 8, (2001) 2170.
- [18] Charlton, L.A., Holmes, J.A., Hicks, H.R., et al., Journal Comp. Phys., 63, (1986) 107.
- [19] Leboeuf, J-N. G., and Kurita, G., JAERI-Research, 98-010, 1998.
- [20] Pogutse, O.P., and Yurchenko, E.I., Sov. J. Plasma Phys., 3, (1977) 283.
- [21] Kurita, G., Azumi, M., Takizuka, T., et al., Nucl. Fusion, 26, (1986) 449.